Reorientational versus Kerr dark and gray solitary waves using modulation theory

Gaetano Assanto,[1] T. R. Marchant,[2] Antonmaria A. Minzoni,[3] and Noel F. Smyth[4]

[1]*NooEL, Nonlinear Optics and OptoElectronics Lab, University of Rome "Roma Tre," Via della Vasca Navale 84, 00146 Rome, Italy*

[2]*School of Mathematics and Applied Statistics, University of Wollongong, Northfields Avenue, Wollongong, New South Wales 2522, Australia*

[3]*Fenomenos Nonlineales y Mecánica (FENOMEC), Department of Mathematics and Mechanics, Instituto de Investigación en Matemáticas Aplicádas y Sistemas, Universidad Nacional Autónoma de México, 01000 México D.F., México*

[4]*School of Mathematics and Maxwell Institute for Mathematical Sciences, University of Edinburgh, Edinburgh EH9 3JZ, Scotland, UK*

(Received 23 September 2011; published 9 December 2011)

We develop a modulation theory model based on a Lagrangian formulation to investigate the evolution of dark and gray optical spatial solitary waves for both the defocusing nonlinear Schrödinger (NLS) equation and the nematicon equations describing nonlinear beams, nematicons, in self-defocusing nematic liquid crystals. Since it has an exact soliton solution, the defocusing NLS equation is used as a test bed for the modulation theory applied to the nematicon equations, which have no exact solitary wave solution. We find that the evolution of dark and gray NLS solitons, as well as nematicons, is entirely driven by the emission of diffractive radiation, in contrast to the evolution of bright NLS solitons and bright nematicons. Moreover, the steady nematicon profile is nonmonotonic due to the long-range nonlocality associated with the perturbation of the optic axis. Excellent agreement is obtained with numerical solutions of both the defocusing NLS and nematicon equations. The comparisons for the nematicon solutions raise a number of subtle issues relating to the definition and measurement of the width of a dark or gray nematicon.

DOI: 10.1103/PhysRevE.84.066602 PACS number(s): 05.45.Yv, 42.65.Tg, 42.70.Df

I. INTRODUCTION

The nonlinear Schrödinger (NLS) equation

$$i\frac{\partial u}{\partial z}+\frac{1}{2}\frac{\partial^2 u}{\partial x^2}+|u|^2u=0 \tag{1}$$

is a nonlinear wave equation arising in a broad range of physical settings, including water waves and nonlinear optics [1,2]. This equation is of special interest because it possesses an exact solution in terms of the inverse scattering transform [1], which implies that it has soliton (rather than just solitary wave) solutions, an infinite number of conservation laws, etc. The distinction between solitary wave and soliton solutions is that when any number of solitons interact they do not change form, and the only outcome of the interaction is a phase shift. Various generalizations of the NLS equation (1) arise in optics [2] and possess solitary wave, but not soliton, solutions, including nonlinear beams in reorientational media such as nematic liquid crystals, which is of particular relevance to the present work [3–5].

The most common version of the NLS equation (1) contains the so-called Kerr self-focusing term, by which a higher intensity corresponds to a proportionally higher refractive index, so that an optical beam self-focuses [1,2,6]. When Kerr self-focusing balances diffraction the solution is referred to as a bright soliton as it is an isolated self-confined beam on a dark background of zero intensity. Conversely, if the sign of the nonlinearity in Eq. (1) is reversed, the defocusing NLS equation

$$i\frac{\partial u}{\partial z}+\frac{1}{2}\frac{\partial^2 u}{\partial x^2}-|u|^2u=0 \tag{2}$$

results, which models a medium for which there is a reduction in refractive index wherever there is an increased intensity, leading to self-defocusing of light beams and, eventually, to the formation of dark and gray soliton solutions, i.e., propagation invariant dips on a finite background level [2]. For a dark soliton the intensity goes to zero on axis, while for a gray soliton it reduces to a nonzero level below the background. In this work we consider dark and gray NLS solitons and dark and gray nematicons, the latter being the solitary wave solutions of the self-defocusing nematicon equations. While nematic liquid crystals are self-focusing, the addition of suitable dyes (e.g., azo molecules) can turn them into defocusing media [7]. Modulation theory will be used to find a variational approximation to the steady dark and gray nematicon solutions. In addition, the same approach will be used to analyze how dark and gray nematicons evolve from a fairly general initial condition. Neither the focusing nor the defocusing nematicon equations possess an exact solitary wave solution. Modulation theory has proven to be a useful approximate technique for analyzing the evolution of bright solitary waves governed by equations, particularly focusing NLS-type equations, which do not possess an exact solution for these solitary waves. While it has been extensively applied to focusing NLS-type equations, it has not been applied to the equations governing nonlinear beam propagation in defocusing media. Modulation theory is based on the choice of a suitable trial function for the unknown solitary wave profile in a Lagrangian formulation of the governing equations [8]. For NLS equations that do possess an exact solitary wave solution, this modulation theory approach reduces to standard perturbation theory [8]. Modulation theory has proven to be a successful approximate analytical theory providing solutions in excellent agreement with numerical [9,10] and experimental results [5,11,12], even for the refraction of nematicons in nonuniform media [12–15]. In addition, it has been found to give excellent results for more complicated structures, such as undular bores [16] and optical vortices [17–20]. An advantage of using modulation theory to develop approximate solutions is

that the diffractive radiation shed when a solitary wave evolves can be incorporated [8,9,21]. Accounting for this diffractive radiation is crucial in the present work as the evolution of dark and gray solitary waves is fundamentally determined by it. In previous studies using averaged Lagrangian techniques dark solitons evolved due to perturbation terms added to the defocusing NLS equation (2), so that radiation played little role [22,23]. In contrast to the evolution of a bright NLS soliton [8], however, ignoring this radiative loss yields modulation equations that show no evolution. To understand the role of radiation on the evolution of a dark (gray) nematicon, we first develop the required tools and understanding for the simpler defocusing NLS equation. Indeed, for both the defocusing NLS and nematicon equations the modulation equations show the evolution of an initial condition to dark and gray solitary waves and provide simple exact solutions in excellent agreement with numerical ones.

II. DARK AND GRAY NLS SOLITONS

Before considering the dark and gray solitary waves of the defocusing nematicon equations, let us consider the $(1+1)$-D Kerr case, e.g., the defocusing NLS equation (2). This has the soliton solution

$$u = [B\tanh B(x - Az) + iA]e^{-iu_0^2 z}, \quad A^2 + B^2 = u_0^2, \tag{3}$$

which is dark for $A = 0$ and $B = u_0$ and gray for $A \neq 0$ [2]. While the defocusing NLS equation yields exact dark and gray solitons, the defocusing nematicon equations to be considered in Sec. IV do not possess such solutions. In the absence of exact solutions, a useful approach consists of using trial functions in a variational formulation of the governing equations [8,9,24]. In the limit of a slowly varying wave train, this variational approach is the same as Whitham modulation theory [1]. A commonly used trial function is the chirped solitary wave of Anderson [24], which gives good results for a wide variety of NLS-type equations [25]. However, a drawback of this chirped form is that there is no way to include radiative losses, so that the solitary wave under this approximation does not evolve to a steady state. An alternative approach accounting for this radiative loss has been developed [8,9,21], with the radiative terms derived from perturbed inverse scattering [8]. The form of these terms has independently been obtained using standard soliton perturbation theory [26–28].

The NLS equation (2) has the Lagrangian

$$L = i(u^* u_z - u u_z^*) - |u_x|^2 - |u|^4 - u_0^4 \tag{4}$$

with the asterisk superscript denoting the complex conjugate. To find approximations to the dark and gray NLS soliton solutions, we use the trial function

$$u = \left(B\tanh\frac{x-\xi}{w} + iA\right)e^{-iu_0^2 z}, \quad A^2 + B^2 = u_0^2, \tag{5}$$

which is based on the exact solution (3), as in Refs. [22,23]. The parameters w, A, and B are now functions of z. The waist is w_0 at $z = 0$ and $w_0 \neq 1/B$ in general, so that the initial condition will evolve in a self-similar fashion to the exact soliton (3). The trial function (5) does not contain a shelf term, as for an evolving bright NLS soliton [8]. The long-wavelength radiation shed by an evolving soliton has low group velocity and so accumulates under the soliton, forming a shelf [8,28]. If such a shelf term were included in the trial function (5), at first order it would give zero contribution as all integrals involving the even shelf and the odd dark soliton integrate to zero in the averaged Lagrangian. The "chirp" variational method [24] cannot be used for the dark or gray solitons as the integrals involving the chirp are divergent. Moreover, since it will be found that the dark (gray) soliton evolution is driven completely by the emitted diffractive radiation, which cannot be incorporated in the chirp method, this method is unsuitable for analyzing the evolution of dark or gray solitons, even if no divergent integrals were involved. Substituting the trial function (5) into the Lagrangian (4) and averaging by integrating in x from $-\infty$ to ∞ results in the averaged Lagrangian

$$\mathcal{L} = -4\left(AB - u_0^2\tan^{-1}\frac{B}{A}\right)\xi' - \frac{4}{3}\frac{B^2}{w} - \frac{4}{3}B^4 w. \tag{6}$$

It should be noted that the $\tan^{-1} B/A$ term has been added to disentangle the background carrier wave from the actual dark soliton [22,23].

Variations of the averaged Lagrangian (6) with respect to B, w, and ξ give

$$\frac{d\xi}{dz} = \frac{A}{3Bw} + \frac{2}{3}ABw, \tag{7}$$

$$w = B^{-1}, \tag{8}$$

$$\frac{dB}{dz} = 0. \tag{9}$$

The variational equations then give the exact dark soliton solution (3) and no evolution occurs, because the radiation loss has not been included and so the parameters of (5) cannot adjust. This behavior is unlike that for the bright NLS soliton for which the amplitude and waist undergo a harmonic oscillation without evolving to a steady state when radiation loss is ignored [8]. The form of this radiation loss and the consequent modification of the variational equations will be considered next.

III. RADIATION LOSS FOR DARK AND GRAY NLS SOLITONS

The radiation shed by an evolving dark or gray soliton has an amplitude much lower than that of the soliton. Hence, it is governed by the NLS equation (2) linearized about the background carrier wave. Let us linearize with

$$u = u_0 e^{-iu_0^2 z} + u_1 e^{-iu_0^2 z}, \tag{10}$$

where $|u_1| \ll |u_0|$. Substituting this linearized expansion into the NLS equation (2) and neglecting terms quadratic and higher in u_1 results in

$$i\frac{\partial u_1}{\partial z} + \frac{1}{2}\frac{\partial^2 u_1}{\partial x^2} - u_0^2(u_1 + u_1^*) = 0. \tag{11}$$

This linear equation will be solved using Laplace transforms. Before doing this, let us consider what is needed to calculate the radiation loss from the dark soliton, dominated by mass loss as for bright solitons [8].

The NLS equation (2) has the mass conservation equation

$$i\frac{\partial}{\partial z}(|u|^2-|u_0|^2)+\frac{1}{2}(u^*u_x-uu_x^*)=0. \tag{12}$$

As for a bright NLS soliton, long-wavelength linear radiation has low group velocity, so it forms a shelf of size ℓ under the evolving dark soliton [8]. The existence of this radiation shelf has also been proven using perturbation theory [28]. Integrating from the edge of the shelf at $\xi+\ell/2$ to ∞ gives the mass lost to radiation, which propagates to the right of the soliton as

$$\frac{d}{dz}\int_{\xi+\ell/2}^{\infty}(|u|^2-|u_0|^2)\,dx = \mathrm{Im}\,u^*u_x|_{x=\xi+\ell/2}=\mathrm{Im}(u_0+u_1^*)u_{1x}|_{x=\xi+\ell/2}, \tag{13}$$

on using the linearization (11). A similar expression holds for radiation propagating to the left. We then just need to determine $\mathrm{Im}(u_1^*u_{1x})$ at $x=\xi+\ell/2$ to calculate the soliton mass lost to shed radiation.

To solve the linearized radiation equation (11) it is convenient to convert it into a system of equations by setting $u_1=f+ig$, where f and g are real. Then

$$\frac{\partial g}{\partial z}-\frac{1}{2}\frac{\partial^2 f}{\partial x^2}+2u_0^2 f=0,\quad \frac{\partial f}{\partial z}+\frac{1}{2}\frac{\partial^2 g}{\partial x^2}=0. \tag{14}$$

This system can be solved using Laplace transforms, on noting that there is no initial radiation, so that $f=g=0$ at $z=0$. The radiation is matched to the shelf at $x=\xi+\ell/2$. If the shelf has height r at $x=\xi+\ell/2$, then from the expansion (10) we obtain

$$u_1=re^{i\varphi}e^{iu_0^2z}\quad\text{at}\quad x=\xi+\ell/2, \tag{15}$$

where φ is the phase of the shelf at $x=\xi+\ell/2$. The shelf height r can be estimated by noting that the mass in the shelf at z is

$$\int_{-\infty}^{\infty}(|u|^2-|u_0|^2)\,dx=-2B^2w. \tag{16}$$

The shelf of size ℓ contains the excess mass that the soliton sheds in order to reach its steady-state mass $-2B_f^2w_f$ [21]. Hence

$$r^2=\frac{2B^2w-2B_f^2w_f}{\ell}. \tag{17}$$

On taking Laplace transforms of the system (14) the resulting linear system has four eigenvalues. The two that give decay as $x\to\infty$ are

$$\lambda_{\pm}=-\sqrt{2}\sqrt{u_0^2\pm\sqrt{u_0^4-s^2}}, \tag{18}$$

where s is the Laplace transform variable. Expanding for large s shows that the root λ_+ corresponds to incoming waves, so it is neglected. It is then found that

$$\bar{u}_1=\bar{f}+i\bar{g}=D\left(i-\frac{\lambda_-^2}{2s}\right)e^{\lambda_- x}, \tag{19}$$

where the overbar denotes the Laplace transform, D is an integration constant, and λ_- is given by (18). It is not possible to invert this Laplace transform, but a large z expansion, i.e., a small s expansion, can provide the asymptotic behavior of the radiation. For $s\to 0$

$$\bar{u}_{1x}\sim-\frac{s}{u_0}\bar{u}_1, \tag{20}$$

so that

$$u_{1x}\sim-u_0^{-1}u_{1z} \tag{21}$$

as $z\to\infty$. Substituting this asymptotic limit for the radiation into (13) and using the boundary condition (15) we find

$$\frac{d}{dz}\int_{\xi+\ell/2}^{\infty}(|u|^2-|u_0|^2)\,dx=-u_0r^2, \tag{22}$$

on noting that the dominant z derivative comes from the phase iu_0^2z in Eq. (15) and that the contribution of the u_{1z} term alone averages to zero. Finally, adding the loss (22) and its counterpart in $x<\xi-\ell/2$ to the rate of change of the soliton mass (16) gives the mass conservation equation with radiation loss

$$\frac{d}{dz}(B^2w)=-2u_0\frac{B^2w-B_f^2w_f}{\ell}. \tag{23}$$

The variational equation (9) shows that the depth B of the dark (gray) soliton is fixed. Let us denote fixed-point values by the subscript f. The mass-loss equation (23) can then be integrated to provide

$$w=w_f+(w_0-w_f)e^{-2u_0z/\ell},\quad\text{where}\quad w_f=B_0^{-1}, \tag{24}$$

and $w=w_0$ and $B=B_0$ at $z=0$. The steady-state value w_f is just the relation for the exact dark (gray) soliton solution (3). Finally, the modulation equations for the evolution of a dark (gray) NLS soliton have a simple analytical solution, unlike those for the evolution of a bright NLS soliton [8].

IV. DARK AND GRAY NEMATICONS

Let us now apply the theory developed for the defocusing NLS equation to the defocusing nematicon equations:

$$i\frac{\partial u}{\partial z}+\frac{1}{2}\frac{\partial^2 u}{\partial x^2}-2\theta u=0, \tag{25}$$

$$\nu\frac{\partial^2\theta}{\partial x^2}-2q\theta=-2|u|^2, \tag{26}$$

with u the envelope of the electric field of the light beam and θ the angular orientation of the optic axis (or director) of the nematic liquid crystals with respect to the beam wave vector along z [4,5]. The dark and gray nematicons will form on a linear carrier wave. The linear solution of the nematicon equations (25) and (26) is

$$u=u_0e^{-2iu_0^2z/q},\quad \theta=\frac{u_0^2}{q}. \tag{27}$$

Hence, the system (25) and (26) has the Lagrangian

$$L=i(u^*u_z-uu_z^*)-|u_x|^2-4\theta|u|^2+\nu\theta_x^2+2q\theta^2-\frac{2u_0^4}{q}. \tag{28}$$

A trial function for a modulation theory of the electric field u can be developed in analogy with that for the defocusing

NLS equation (Sec. II). A suitable function matching with the carrier wave is

$$u = \left(B \tanh \frac{x-\xi}{w} + iA \right) e^{-2iu_0^2 z/q}, \quad B^2 + A^2 = u_0^2. \tag{29}$$

A trial function for θ needs more care as it must match with the solution of the director reorientation equation (26) as $x \to \pm\infty$, based on u given by (29). Such a suitable trial function is

$$\theta = \frac{1}{q} \left(\alpha^2 \tanh^2 \frac{x-\xi}{\beta} + \gamma^2 \right), \quad \alpha^2 + \gamma^2 = u_0^2. \tag{30}$$

Due to nonlocality, the width of the director distribution is larger than that of the beam and $\beta \gg w$ in the highly nonlocal limit (ν large) [4,29]. As for the dark and gray solitons of the defocusing NLS equation, the trial functions (29) and (30) are now substituted into the Lagrangian (28), which is then averaged by integrating in x from $-\infty$ to ∞ (see Ref. [1]), resulting in

$$\mathcal{L} = -4 \left(AB - u_0^2 \tan^{-1} \frac{B}{A} \right) \xi' - \frac{4}{3} \frac{B^2}{w} - \frac{4\sqrt{\pi} C_1 C_2 B^2 \alpha^2 \beta w}{q \sqrt{C_1^2 \beta^2 + C_2^2 w^2}} + \frac{16\nu}{15} \frac{\alpha^4}{q^2 \beta} + \frac{8}{3q} \alpha^4 \beta. \tag{31}$$

Here

$$C_1 = \frac{2\sqrt{6}}{\pi^{3/2}} \quad \text{and} \quad C_2 = \frac{2}{\sqrt{\pi}} \tag{32}$$

in the limit ν large, which is the relevant case for light beams in nematic liquid crystals [7,29]. Again, the $\tan^{-1} B/A$ term has been added to subtract out the momentum of the carrier wave [22,23].

Variations with respect to B, ξ, α, and β give

$$\frac{B}{A} \frac{d\xi}{dz} = \frac{1}{3w} + \frac{\sqrt{\pi} C_1 C_2 \alpha^2 \beta w}{q \sqrt{C_1^2 \beta^2 + C_2^2 w^2}}, \tag{33}$$

$$\frac{dB}{dz} = 0, \tag{34}$$

$$\frac{4}{3} \left(1 + \frac{2\nu}{5q\beta^2} \right) \alpha^2 = \frac{\sqrt{\pi} C_1 C_2 B^2 w}{\sqrt{C_1^2 \beta^2 + C_2^2 w^2}}, \tag{35}$$

and

$$\frac{2}{3} \left(1 - \frac{2\nu}{5q\beta^2} \right) \alpha^2 = \frac{\sqrt{\pi} C_1 C_2^3 B^2 w^3}{\left(C_1^2 \beta^2 + C_2^2 w^2 \right)^{3/2}}, \tag{36}$$

respectively. The last two modulation equations can be solved to provide

$$2C_1^2 \beta^2 = \frac{2\nu C_1^2}{5q} + C_2^2 w^2 + \left[\left(\frac{2\nu C_1^2}{5q} + C_2^2 w^2 \right)^2 + \frac{24\nu C_1^2 C_2^2 w^2}{5q} \right]^{1/2}. \tag{37}$$

Variations with respect to w can also be found. However, as for the defocusing NLS equation of Sec. II, these variations only lead to the fixed-point, or steady dark nematicon, relation as loss to shed radiation has not yet been included. Mass loss to radiation again drives the evolution of a dark or gray nematicon. Variations with respect to w give

$$w_f^{-2} = \frac{3\sqrt{\pi} C_1^3 C_2 \alpha_f^2 \beta_f^3}{q \left(C_1^2 \beta_f^2 + C_2^2 w_f^2 \right)^{3/2}}. \tag{38}$$

The steady-state nematicon is found by solving the transcendental equations (35), (37), and (38) for the quantities α_f, β_f, and w_f.

V. RADIATION LOSS FOR DARK AND GRAY NEMATICONS

As previously noted, the effect of the radiation lost as the dark nematicon evolves must be included in the modulation equations of the previous section in order for the solution to evolve to a fixed point, giving the steady-state dark nematicon. The simplest way to include radiation loss in the modulation equations is again to consider the mass equation (13), which also holds for the dark nematicon equations (25) and (26). As the amplitude of the shed radiation is much smaller than that of the nematicon (as for the NLS equation of Sec. III), away from the nematicon we have

$$u = u_0 e^{-2iu_0^2 z/q} + u_1 e^{-2iu_0^2 z/q}, \tag{39}$$

$$\theta = \frac{u_0^2}{q} + \theta_1, \tag{40}$$

with $|u_1| \ll u_0$ and $|\theta_1| \ll u_0^2/q$. The perturbation u_1 is the shed radiation, with θ_1 being the effect of the radiation on the orientation of the optic axis. With these linearizations the same mass-loss expression (13) applies.

Substituting the linearizations (39) and (40) into the nematicon equations (25) and (26), we have at first order

$$i \frac{\partial u_1}{\partial z} + \frac{1}{2} \frac{\partial^2 u_1}{\partial x^2} - 2u_0 \theta_1 = 0, \tag{41}$$

$$\nu \frac{\partial^2 \theta_1}{\partial x^2} - 2q\theta_1 = -2u_0 (u_1 + u_1^*). \tag{42}$$

The solution of these equations for the shed radiation is then matched at $x = \xi \pm \ell/2$ with the shelf of radiation under the nematicon, so that at $x = \xi \pm \ell/2$, $u_1 = |u_1| \exp[i\psi(z)]$, with $\psi(z)$ a slowly varying function (see Ref. [8]), and θ_1 is to be determined consistently due to the equation for θ_1 (42) being elliptic. At $z = 0$, $u_1 = 0$ and $\theta_1 = 0$ as initially there is no radiation. Let us first consider the region $x \geqslant \xi + \ell/2$ to the right of the evolving nematicon. Again, the linear system (41) and (42) is most easily solved by splitting u_1 into real and imaginary parts, $u_1 = f + ig$, where f and g are real. We thus have

$$\frac{\partial g}{\partial z} - \frac{1}{2} \frac{\partial^2 f}{\partial x^2} + 2u_0 \theta_1 = 0, \tag{43}$$

$$\frac{\partial f}{\partial z} + \frac{1}{2} \frac{\partial^2 g}{\partial x^2} = 0, \tag{44}$$

$$\nu \frac{\partial^2 \theta_1}{\partial x^2} - 2q\theta_1 = -4u_0 f. \tag{45}$$

The boundary conditions for this system are

$$\begin{aligned} f &= f_b = |u_1|\cos\left(\psi + 2u_0^2 z/q\right), \\ g &= g_b = |u_1|\sin\left(\psi + 2u_0^2 z/q\right) \end{aligned} \tag{46}$$

at $x = \xi \pm \ell/2$. The real system (43)–(45) can be solved using Laplace transforms in z. The resulting system can be shown to have solutions that decay for $x > 0$. As the Laplace transform solution cannot be inverted exactly, it is expanded for small transform variable s, which is equivalent to large z, to obtain the large z behavior of the shed radiation. In this manner we obtain

$$\mathbf{a} = P\mathbf{b}e^{-\lambda_1(x-x_0)} + Q\mathbf{b}^* e^{-\lambda_1^*(x-x_0)} + R\mathbf{c}, \tag{47}$$

where $x_0 = \xi + \ell/2$,

$$\begin{aligned} \mathbf{a} &= (\bar{f},\bar{g},\bar{\theta}_1)^T,\ \mathbf{b} = \left(1, \frac{2s}{\lambda_1^2}, \lambda_1\right)^T, \\ \mathbf{c} &= \left(1, -\frac{2u_0^2}{qs}, -\frac{2u_0}{q\nu s^2}\right)^T, \end{aligned} \tag{48}$$

and

$$\lambda_1 = e^{i\pi/4}\left(\frac{q}{\nu} + \sqrt{\frac{q^2}{\nu^2} + \frac{16u_0^2}{\nu}}\right)^{1/2} \tag{49}$$

for ν large. Here the overbar again denotes the Laplace transform, and P, Q, and R are constants of integration, which are functions of s. The constants of integration are determined from the boundary conditions after Eq. (42), giving

$$R = \frac{qs}{2u_0^2}\bar{g}_b, \quad P = Q = \frac{\bar{f}_b}{2} - \frac{qs}{4u_0^2}\bar{g}_b. \tag{50}$$

Unlike the dark NLS soliton of Sec. III, the contribution to the mass flux in Eq. (13) from $u_0 u_{1x}$ is zero, so that the mass lost to radiation that propagates to the right of the nematicon is

$$\frac{d}{dz}\int_{\xi+\ell/2}^{\infty} (|u|^2 - |u_0|^2)\, dx = g f_x|_{x=\xi+\ell/2}. \tag{51}$$

The large z (small s) solution (47) is now used to evaluate the flux term in this mass-loss equation. The terms involving the s multiplicative factor are approximated to leading order in terms of the z derivative of g at the boundary, as in Eq. (21). These then give a contribution proportional to g^2, which is then averaged over the fast $2u_0^2 z/q$ time scale imposed by the boundary condition on g in Eq. (46). In a similar manner to the derivation of the mass loss (22) for the dark NLS soliton, we find that after this averaging the final result for the equation of mass conservation for the dark (gray) nematicon, including loss to diffractive radiation, is

$$\begin{aligned} &\frac{d}{dz}(B^2 w) = -\Gamma\frac{B^2 w - B_f^2 w_f}{\ell}, \\ &\text{where}\quad \Gamma = \frac{1}{2}\left(\frac{q}{\nu} + \sqrt{\frac{q^2}{\nu^2} + \frac{16u_0^2}{\nu}}\right)^{1/2}. \end{aligned} \tag{52}$$

As for the dark soliton of Sec. II, the depth B of the dark (gray) nematicon is fixed from the variational equation (34), so the mass-loss equation (52) can be integrated to give

$$w = w_f + (w_0 - w_f)e^{-\Gamma z/\ell}, \tag{53}$$

where w_0 is the initial value of w. The modulation equations for the evolution of a dark (gray) nematicon comprise the explicit solution for w (53), together with the transcendental equations (35) and (37) for α and β. Hence the solution for w has the same simple form as for the defocusing NLS equation. There is no simple expression for the fixed-point width w_f, however, as the fixed-point relation (38) has to be solved in conjunction with the algebraic equations (35) and (37).

VI. RESULTS AND DISCUSSION

The numerical solutions of the defocusing NLS and nematicon equations (2), (25), and (26), respectively, were obtained using a hybrid Runge-Kutta finite difference scheme for the NLS or NLS-type equations (2) and (25), and Gauss-Seidel iteration with successive over-relaxation for the director equation (26). The scheme details are described in the Appendix. For all the numerical solutions presented here the discretizations $\Delta x = 0.1$ and $\Delta z = 1 \times 10^{-2}$ were used.

A. Dark and gray NLS solitons

We shall compare results of the modulation theory with numerical solutions for both the width and the position of evolving dark and gray solitons. For the dark and gray NLS solitons, numerical solutions show that the trough depth A and far field amplitude u_0, and hence B, do not evolve and only the width w and the position ξ of the soliton evolve, in agreement with the modulation theory of Sec. II. To obtain these comparisons between numerical solutions and modulation theory, we measure the soliton width at an amplitude $|u| = (u_0 + A)/2$, which is half of its total depth. Such an analytical width is

$$\begin{aligned} w_m &= 2w\tanh^{-1} u_m, \\ \text{where}\quad u_m &= \frac{[(u_0 + A)^2 - A^2]^{\frac{1}{2}}}{2B}. \end{aligned} \tag{54}$$

The modulation solution for the width evolution of the dark and gray NLS solitons is (24). As A and B are constant in the modulation theory, the position (7) can be found explicitly. The width and position of dark and gray NLS solitons are then given by (24) and

$$\begin{aligned} \xi = {} & \frac{2}{3}AB\left[w_f z - \frac{\ell}{2u_0}(w_0 - w_f)e^{-2u_0 z/\ell}\right] \\ & + \frac{A}{3}\left\{z + \frac{\ell}{2u_0}\ln[w_f + (w_0 - w_f)e^{-2u_0 z/\ell}]\right\} - \xi_0, \end{aligned} \tag{55}$$

where

$$\xi_0 = -\frac{2\ell}{3u_0}AB(w_0 - w_f) + \frac{A\ell}{3u_0}\ln(w_0). \tag{56}$$

In the following discussion of results for dark and gray Kerr solitons and nematicons the quantity w shall be referred to as

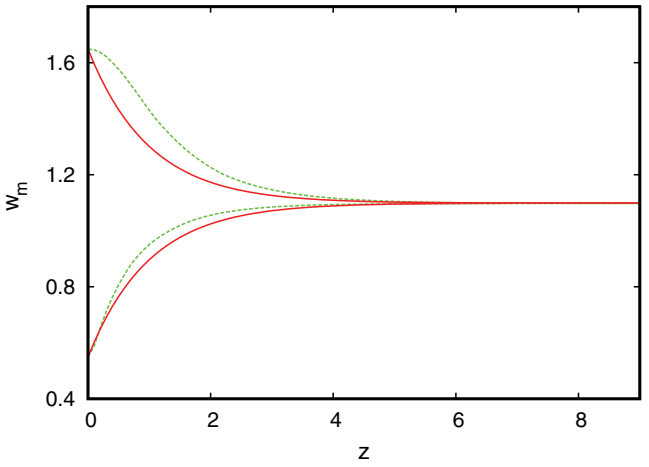

FIG. 1. (Color online) The beam half-waist vs propagation distance, w_m vs z, for a dark NLS soliton. Shown are the analytical solution from modulation theory [solid lines (red)] and numerical solution [dashed lines (green)]. The upper pair of curves is for $w_0 = 1.5$ and the lower pair for $w_0 = 0.5$. The other parameters are $A = 0$ and $B = 1$.

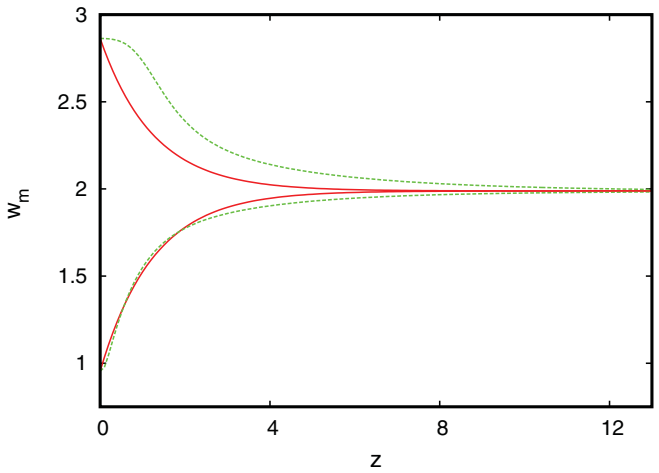

FIG. 2. (Color online) The beam half-waist vs propagation distance, w_m vs z, for a gray NLS soliton. The analytical solution from modulation theory [solid lines (red)] and the numerical solution [dashed lines (green)] are graphed. The upper pair of curves is for $w_0 = 1.8$ and the lower pair for $w_0 = 0.6$. The other parameters are $A = 0.6$ and $B = 0.8$.

the waist and w_m as the half-waist. The shelf width ℓ [28] was chosen to be $\ell = w_f$ as this gives the correct decay rate of the soliton waist onto the steady-state value for a broad range of initial conditions. This value differs from that for bright NLS beam evolution, for which $\ell \approx 3w_f$ [8].

Figure 1 shows the beam half-waist versus propagation distance, w_m versus z, for a dark NLS soliton. Two examples are shown for the initial values $w_0 = 1.5$ and $w_0 = 0.5$. The other parameters are $A = 0$ and $B = 1$, so the background amplitude is $u_0 = 1$. In this example the final waist is $w_f = B^{-1} = 1$, with the initial half-waists being $w_{m0} = 1.68$ and $w_{m0} = 0.549$ and the final half-waist being $w_{mf} = 1.10$. The figure shows that for both initial conditions the half-waist relaxes quickly to the steady-state value, being within 1% of the steady-state value by $z \approx 5.8$. The results also confirm the modulation theory prediction that A and B remain constant, as analytical and numerical values of the steady-state half-waist differ by less than 0.1%. It can be seen that, for the initial condition $w_0 = 1.5$, initially the numerical half-waist does not change greatly. The soliton undergoes some initial internal rearrangement that is not captured by the modulation trial function (5). However, the final decay rate of the soliton onto the steady state is well captured by the modulation theory. A dark NLS soliton remains stationary at the initial location $\xi = 0$ for all z.

Figure 2 shows the beam half-waist versus propagation distance, w_m versus z, for a gray NLS soliton. Two examples are shown for the initial conditions $w_0 = 1.8$ and $w_0 = 0.6$. The other parameters are $A = 0.6$ and $B = 0.8$, so again the background amplitude is $u_0 = 1$. For this example the final waist is $w_f = B^{-1} = 1.25$, the initial half-waists are $w_{m0} = 2.86$ and $w_{m0} = 0.954$, and the final half-waists are $w_{mf} = 1.99$. The figure shows that for both examples the half-waist relaxes quickly onto the steady-state value, being within 1% of it by $z \approx 9.4$. The analytical and numerical values of the steady-state half-waist differ by less than 0.3%, which again confirms the accuracy of the modulation equations and their prediction that the depth of a gray soliton does not change, so that A and B are constant. For the wide initial beam there is again some initial reshaping that is not well captured by the modulation trial function (5). However, the comparison is still very good, with the final decay rate of the solitons onto the steady state well predicted by the modulation theory.

Figure 3(a) shows the beam position versus propagation distance, ξ versus z, while Fig. 3(b) shows the beam velocity versus propagation distance, ξ' versus z, for a gray NLS soliton. The same two examples considered in Fig. 2 are displayed, for which $w_0 = 1.8$ and $w_0 = 0.6$. The initial displacement of the soliton for $z \ll 1$ is (55)

$$\xi = Az - \frac{AB\ell}{6u_0}\ln(B) - \xi_0 + O(z^2), \tag{57}$$

which shows that the initial velocity differs little from its steady-state value A. The modulation theory then explains the small change in the velocity of the soliton seen in Fig. 3(b). Figure 3(a) shows that the difference between the analytical and numerical positions, during the soliton evolution, is very small, as expected since the difference in velocity between the two solutions is small. At $z = 13$ the position difference is less than 1%, confirming the excellent comparison for all z values. Figure 3(b) shows that there are some initial differences between the analytical and numerical velocities, but the velocities settle down quickly to the steady-state values by $z \approx 5$. The numerical steady-state velocities are about 4% less than the analytical values of $\xi' = A = 0.6$. The relatively large initial differences between the analytical and numerical velocities are associated with initial rearrangements of the shape of the soliton, which are not captured by the modulation theory.

B. Dark and gray nematicons

A major difference between the evolution of a dark or gray NLS soliton and a dark or gray nematicon is the amount of diffractive radiation produced as they evolve. This is illustrated in Fig. 4, where the greater amount of radiation for the evolving

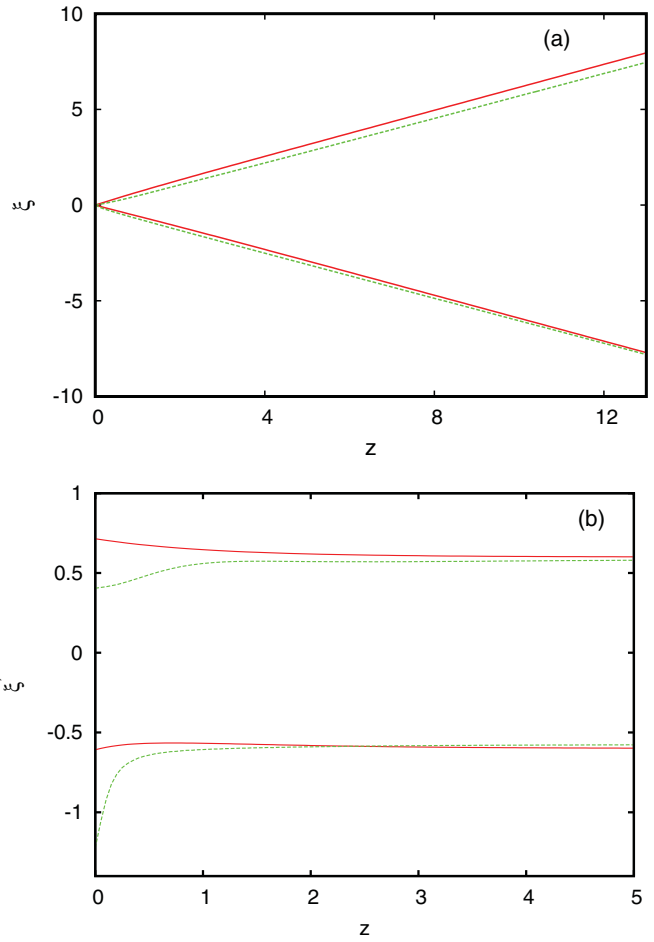

FIG. 3. (Color online) (a) Beam position vs propagation distance, ξ vs z, and (b) beam velocity vs propagation distance, ξ' vs z, for a gray NLS soliton. The analytical solution from modulation theory [solid lines (red)] and the numerical solution [dashed lines (green)] are shown. The upper pair of curves is for $w_0 = 1.8$ and the lower pair is for $w_0 = 0.6$, but with $-\xi$ or -ξ' shown. The other parameters are $A = 0.6$ and $B = 0.8$.

nematicon is clearly visible. The shelf of low wave-number radiation under the dark nematicon can also be seen in this figure as the beam has been shifted off $|u| = 0$, in agreement with theory [28]. The interaction between the nematicon, shelf and radiation changes the nematicon waist in a periodic manner as waves are periodically shed from the edge of the shelf.

The other major difference between a dark or gray Kerr soliton and a dark or gray nematicon is visible in Fig. 5. The steady dark (gray) NLS soliton (3) has a monotonic profile on either side of the notch, while the steady nematicon has two humps, these humps having the same extent as the transverse distribution of the molecular director, i.e., the (extraordinary) refractive index profile. The humps are standing waves trapped by the director profile, and their existence can be explained by linearizing the nematicon equations (25) and (26). The linearized equations (41) and (42) around the background level for the radiation have a steady solution of the form

$$u_0 + C\exp[-\mathrm{Re}(\lambda_1)(x - x_0)] \qquad (58)$$

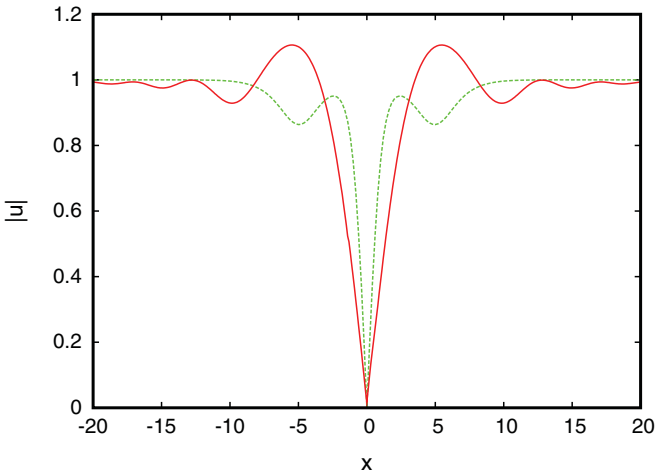

FIG. 4. (Color online) Numerical solutions for NLS dark soliton and dark nematicon. Solution of nematicon equations (25) and (26): solid line (red); solution of NLS equation (2): dashed line (green). The initial parameters are $w = 2$, $B = 1$, $u_0 = 1$, $\nu = 200$, and $q = 2$.

in $x > 0$, with a symmetric solution in $x < 0$, where $\mathrm{Re}(\lambda_1)$ is the rate of decay of the optical axis and is given by (49). The humps in the steady solution of Fig. 5 involve this steady mode, whose width is imposed by the optic axis distribution, typically larger than that of the inner core of the dark nematicon. In Fig. 5 these modes are visible as it is clear that the rate of decay $\mathrm{Re}(\lambda_1)$ matches the decay of the humps. These humps, which cannot occur for the dark NLS soliton but are forced by the optic axis (i.e., index) perturbation via the reorientational nonlinear response, match in a nonlinear fashion to the dark nematicon core.

The existence of the trapped linear mode complicates the comparison of the modulation theory of Secs. IV and V with numerical solutions. The nonlinear transition from the dark nematicon to the trapped mode alters the waist of the

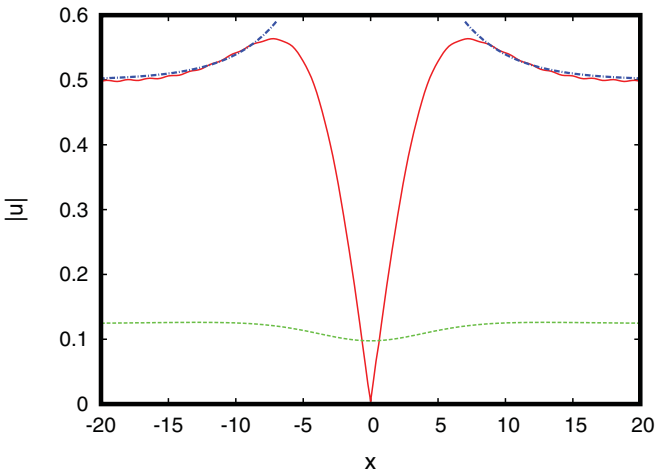

FIG. 5. (Color online) Numerical solutions of nematicon equations (25) and (26). $|u|$: solid line (red); θ: dashed line (green). Eigenfunctions are (58) with $C = 0.09$ and $x_0 = 7$ in $x > 0$ and the symmetric mode in $x < 0$: dot-dashed line (blue). The initial parameters are $w = 2$, $B = 0.5$, $A = 0$, $u_0 = 0.5$, $\nu = 200$, and $q = 2$.

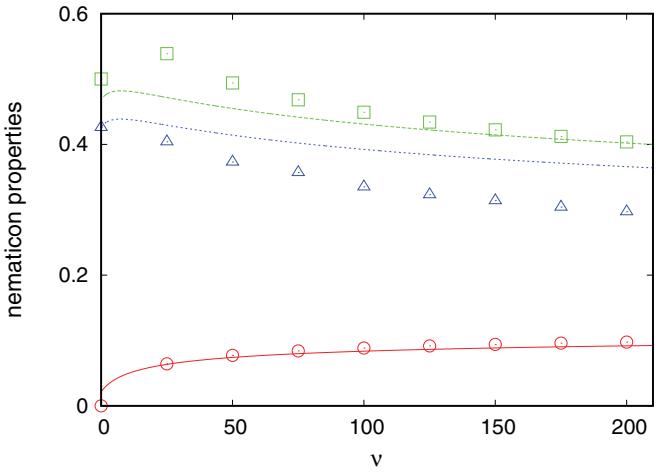

FIG. 6. (Color online) Properties of the steady-state dark nematicon vs the nonlocality ν. Modulation and numerical solutions for the inverse waist w_f^{-1} [solid line and squares (green)], the inverse half-waist w_{mf}^{-1} [dashed lines and triangles (blue)], and the director minimum $\theta(0)$ [dot-dashed lines and circles (red)] are shown. The other parameters are $A = 0$, $u_0 = B = 0.5$, and $q = 2$.

former. While a trapped mode could possibly be incorporated in the trial function (29) [30], this would result in a much more complicated and extensive set of modulation equations, destroying the simplicity of the solution (33), (35), (37), and (53), which will be found to agree well with numerical solutions. So, as well as the half-waist comparisons for the dark NLS soliton, an integral definition of the waist will be used. The mass in the dark (gray) nematicon

$$M = \int_{x_1}^{x_2} \left(u_0^2 - |u|^2\right) dx \tag{59}$$

will be evaluated from numerical data. To avoid the contribution of the trapped mode, x_1 is the value of x to the left of the minimum of the dark nematicon at which $|u| = u_0$ and x_2 is the corresponding point to the right. For the trial function (29) this integral is $2B^2 w$. There are alternative methods for separating out the effect of the trapped linear mode on the beam, for instance, scaling the beam tanh profile to reach the top of the linear mode. These alternatives lead to very similar results to those obtained from the integral (59).

Figure 6 displays the properties of the steady-state dark nematicon versus the nonlocality ν, i.e., the modulation solution (35), (37), and (38), and results from the numerical solution at large $z = 200$. The other parameters are $A = 0$, $u_0 = B = 0.5$, and $q = 2$. Shown are two measures of the inverse waist of the electric field u, w_f^{-1} using the integral (59) and the half-waist w_{mf}^{-1}, and the director minimum $\theta(0) = (u_0^2 - \alpha^2)/q$. The half-waist w_m is measured from the numerical solution at the point at which $|u| = u_0/2 = 0.25$.

In the local limit $\nu \to 0$ the defocusing nematicon equations (25) and (26) reduce to the defocusing NLS equation (2). The modulation solution in this local limit has $\theta(0) = 2.16 \times 10^{-2}$, $w_f^{-1} = 0.468$, and $w_{mf}^{-1} = 0.426$. This can be contrasted with the corresponding exact dark NLS soliton solution, which has $w_f^{-1} = 0.5$, $w_{mf}^{-1} = 0.455$, and $\theta(0) = 0$. The errors in the dark nematicon solution in the local limit are due to the approximation for large ν of the integral of $4\theta|u|^2$ in the Lagrangian (28) for the nematicon equations, which lead to (32). This integral does not have an exact, closed form, and the approximation used is valid in the experimental nonlocal limit [7,29]. For physically realistic experimental scenarios $\nu = O(100)$ [11], in which case the used approximation is accurate.

The waist of the electric field distribution u increases (and the inverse waist decreases) as ν increases, as for a bright nematicon [4,9]. The director profile width (not shown) also increases and becomes much broader than the dark (gray) beam in the nonlocal limit (ν large). This is a characteristic effect of the nonlocality, which results in a broad director (optic axis) response to the electric field, and also occurs for bright nematicons [4,9,29]. The director minimum angle $\theta(0)$ increases as ν increases, again due to nonlocality spreading the director response [4]. The numerical solutions for the waist w and the minimum $\theta(0)$ in director distribution compare very well with the modulation theory predictions over the full range of ν. As ν increases, however, the analytical half-waist w_{mf} is about 20% smaller than the numerical half-waist. This is due to the trapped linear mode seen in Fig. 5, which widens the nematicon at its top end, increasing the half-waist of the combination nematicon beam plus trapped mode. As expected, this widening increases with ν due to the more pronounced director response, resulting in an increasing difference between numerical and modulation half-waists with nonlocality ν. The depth $\theta(0)$ of the director profile is not affected by the trapped linear mode, so the agreement between numerical and modulation solutions is excellent for all ν, except near $\nu = 0$, for the reason stated above. In detail, the modulation solutions for the waist and the director minimum at $\nu = 200$ are $w_f^{-1} = 0.402$, $w_{mf}^{-1} = 0.366$, and $\theta(0) = 9.18 \times 10^{-2}$, while the values from numerical solutions are $w_f^{-1} = 0.404$, $w_{mf}^{-1} = 0.297$, and $\theta(0) = 9.76 \times 10^{-2}$. The inverse waists and director depths are extremely accurate, with differences of less than 5%. However, the difference in the half-waist is much greater, of order 20%, due to the trapped wave effect described above.

Figure 7(a) shows the beam waist, w, versus the propagation distance, z, for a dark nematicon. The waist w is calculated from the numerical solution using the integral (59). Two examples are displayed for the initial values $w_0 = 3$ and $w_0 = 1.8$, the other parameters being $A = 0$, $B = 0.5$, $q = 2$, and $\nu = 200$, so that the carrier amplitude is $u_0 = 0.5$. Figure 7(b) is for the same initial conditions and parameter values but shows the half-waist w_m. The initial half-waists are $w_{m0} = 3.30$ and $w_{m0} = 1.98$. For this example the final waists are $w_f = 2.49$ and $w_{mf} = 2.73$. The integral definition of the waist (59) cannot be used for small z before the shelf has formed. Before the shelf forms $x_1 = -\infty$ and $x_2 = \infty$. As total mass, i.e., the beam mass and that of the shed radiation, is conserved, this integral is constant and provides no evolution in w. The shelf first forms at $z = 6.2$ for $w_0 = 3$ and $z = 2$ for $w_0 = 1.8$, so the numerical curves in Fig. 7(a) begin at these values. The numerical solutions show that, for both initial conditions, the waists undergo damped oscillations as they relax to the steady state, unlike the modulation solutions which exhibit a monotonic decay. The numerical steady-state waists are $w_f = 2.48$ and $w_{mf} = 3.35$. The modulation solution for

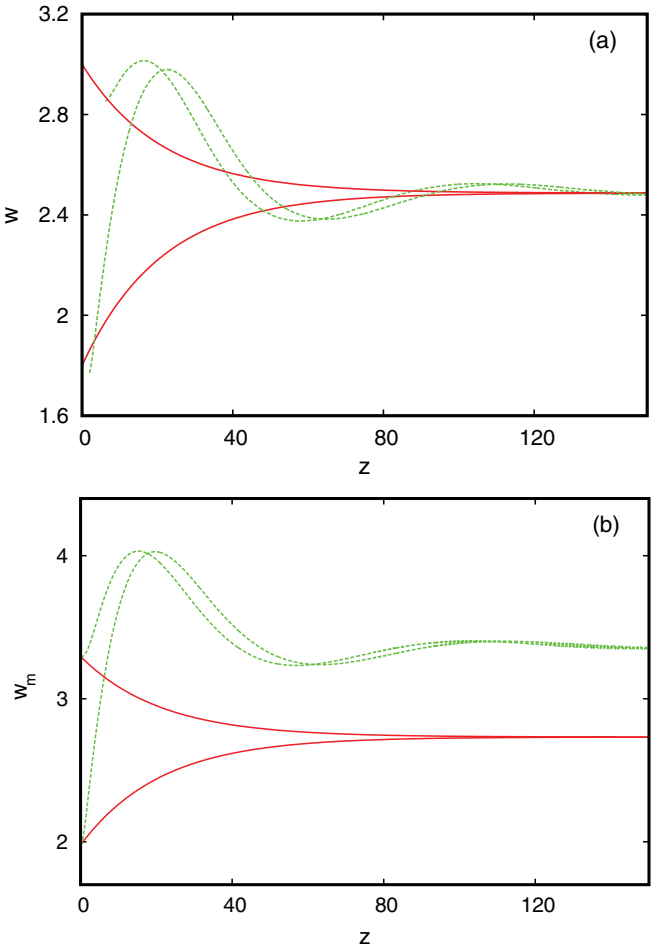

FIG. 7. (Color online) Width evolution for a dark nematicon. Analytical solution from modulation theory [solid lines (red)] and numerical solution [dashed lines (green)] are displayed. In each figure the upper pair of curves is for $w_0 = 3$ and the lower pair for $w_0 = 1.8$. (a) Waist w vs z, (b) half-waist w_m vs z. The other parameters are $A = 0$, $u_0 = B = 0.5$, $q = 2$, and $\nu = 200$.

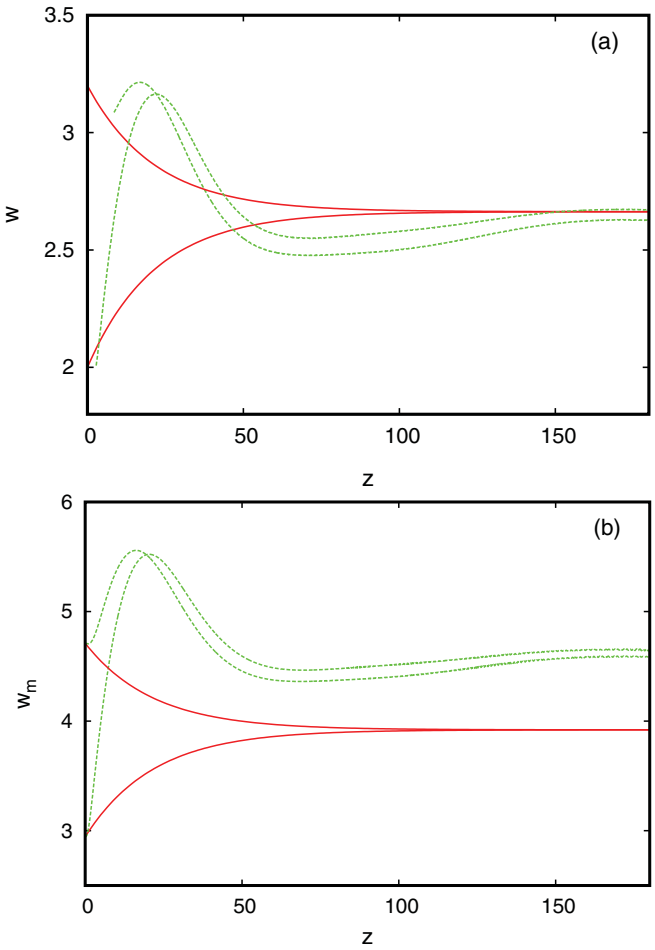

FIG. 8. (Color online) Width evolution for a gray nematicon. Analytical solution from modulation theory [solid lines (red)] and numerical solution [dashed lines (green)] are displayed. In each figure the upper pair of curves is for $w_0 = 3.2$ and the lower pair for $w_0 = 2.0$. (a) Waist w vs z, (b) half-waist w_m vs z. The other parameters are $A = 0.2$, $B = 0.458$, $u_0 = 0.5$, $q = 2$, and $\nu = 200$.

w follows the mean of the numerical damped oscillations for w in Fig. 7(a). The steady integral waist w_f is very close to the analytical solution, but, due to the trapped linear mode, the steady half-waist w_{mf} differs by 20%. The oscillatory nature of the numerical solution is due to the trapped linear mode, as illustrated in Fig. 5. As already discussed, this trapped mode increases the overall waist of the combined beam and linear mode, which is why the agreement in Fig. 7(b) is not as good as that in Fig. 7(a). A proper inclusion of the linear mode in the trial function (29) is not straightforward [30] and would result in a much more involved system of modulation equations. The present modulation equations capture all of the features of the numerical solution. The evolution of the director profile minimum is not shown as it reaches a near steady state for small z because its evolution is not affected by the trapped linear mode of the electric field u. As for the dark NLS soliton, the dark nematicon remains stationary for all z.

Figure 8(a) shows the beam waist, w, versus the propagation distance, z, for a gray nematicon. The waist w is calculated from the numerical solution using the integral (59). Two examples are presented for the initial waists $w_0 = 3.2$ and $w_0 = 2$, the other parameters being $A = 0.2$, $B = 0.458$, $q = 2$, and $\nu = 200$, so that the carrier wave amplitude is $u_0 = 0.5$. Figure 8(b) is for the same initial conditions and parameter values but shows the half-waist w_m. The initial half-waists are then $w_{m0} = 4.71$ and $w_{m0} = 2.94$. For this example the final waists are $w_f = 2.66$ and $w_{mf} = 3.92$. As for the dark case, the integral definition of the waist (59) cannot be used for small z before the shelf has formed. The shelf first forms at $z = 8.5$ for $w_0 = 3.2$ and $z = 2.8$ for $w_0 = 2$, so the numerical curves in Fig. 8(a) begin at these values. The solutions are qualitatively similar to those for the dark nematicon. The numerical waists undergo damped oscillations as they relax to the steady state, unlike the modulation solutions that exhibit a monotonic decay. The numerical steady-state waists are $w_f = 2.66$ and $w_{mf} = 4.63$. The modulation solution for w follows the mean of the numerical damped oscillations for w in Fig. 8(a). The steady integral waist w_f is very close to the analytical solution, but due to the trapped linear mode the steady half-waist w_{mf} differs by about 15%. Once again, as for

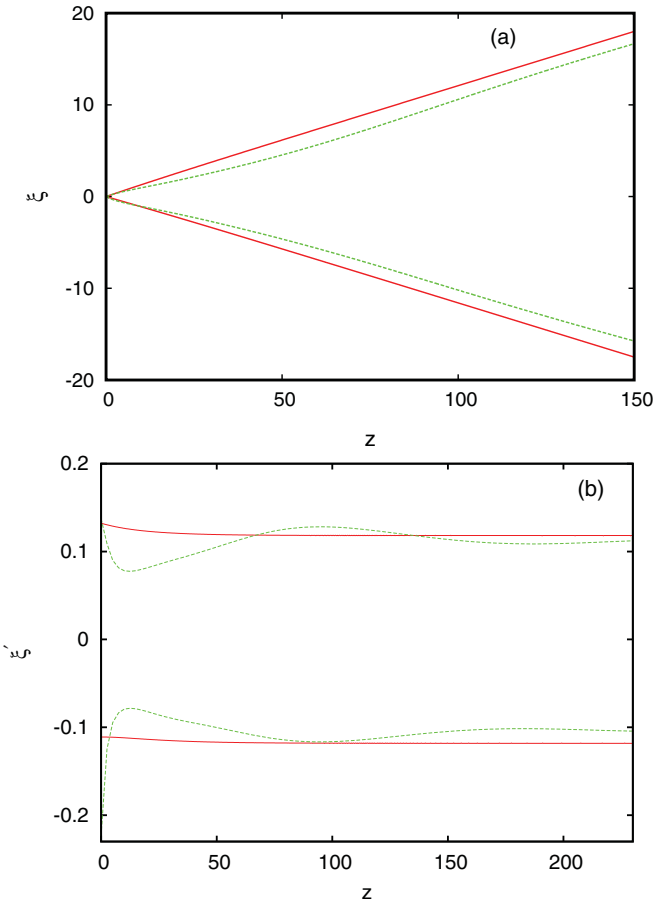

FIG. 9. (Color online) (a) Beam position vs propagation distance, ξ vs z, and (b) beam velocity versus propagation distance, ξ' vs z, for a gray nematicon. The analytical solution from modulation theory [solid lines (red)] and the numerical solution [dashed lines (green)] are shown. The upper pair of curves is for $w_0 = 3.2$, and the lower pair is for $w_0 = 2.0$, but with $-\xi$ or -ξ' shown. The other parameters are $A = 0.2$ and $B = 0.458$, $u_0 = 0.5$, $q = 2$, and $\nu = 200$.

the dark case, the present modulation equations capture all of the features of the numerical solution, except the oscillation, giving instead the mean of the oscillation. The evolution of the director profile minimum is not shown due to its evolution to the steady state over much shorter z. The analytical and numerical values for the director minimum at the steady state are $\theta(0) = 9.55 \times 10^{-2}$ and 1.00×10^{-1}, respectively, a difference of about 5%.

Figure 9(a) shows the beam position versus propagation distance, ξ versus z, while Fig. 9(b) shows the beam velocity versus propagation distance, ξ' versus z, for a gray nematicon. The same two examples considered in Fig. 8 are displayed, for which $w_0 = 3.2$ and $w_0 = 1.8$. In contrast to the NLS case, Eq. (33) for the position ξ must be solved numerically using the explicit solution for w (53) and the solutions for α and β from (35) and (37). Figure 9(b) shows that, for both examples, the velocity of the nematicon settles to its steady-state value at $z \approx 200$. The numerical velocities display oscillations, which are mirrored in the numerical nematicon positions shown in Fig. 9(a). These oscillations are, as for the width oscillations shown in Fig. 8, due to the linear trapped mode. Its attachment points at the nematicon oscillate, which causes the nematicon's position and velocity to oscillate as well. Compared with the gray NLS soliton comparison shown in Fig. 3 the velocity of the gray nematicon has very slow decay to its steady-state value. For the gray NLS soliton considered in Fig. 3(b) the beam reached its steady velocity at about $z = 5$, while the gray nematicon velocity shows some oscillation even past $z = 200$. The position and velocity of the gray NLS soliton do not show much oscillation, due to the lack of the trapped linear mode, as discussed above. At large values of z the analytical and numerical nematicon velocities are $\xi' = 0.118$ and $\xi' = 0.109$, respectively, a difference of 8%. For a gray NLS soliton the steady velocity for the same values of A and B is $\xi' = A = 0.2$. Hence, a gray nematicon travels much more slowly than an equivalent gray NLS soliton. The differences between the analytical and numerical positions are about 10% at $z = 150$. As for the dark NLS soliton of Fig. 3 there are relatively large initial differences in the velocity as given by the numerical solution and modulation theory, particularly for $w_0 = 2$. These are again due to the numerical dark nematicon undergoing initial shape rearrangements not captured by the fixed profile of the modulation theory.

VII. CONCLUSIONS

The dark and gray solitary wave solutions of the defocusing NLS and nematicon equations have been studied in some detail. In particular, a modulation theory has been developed to describe the self-similar evolution of an initial condition to a steady dark or gray solitary wave. While the defocusing NLS equation has an inverse scattering solution, and so is fully understood in principle, it is not clear how use this solution to evaluate in detail the interaction of the dark soliton with the radiation it sheds. Modulation theory was then developed for this equation in order to prepare tools and show their accuracy in the Kerr context in which the dark and gray soliton solutions are known. In contrast to the evolution of bright solitons in Kerr and in reorientational media, this evolution was found to be totally dominated by the diffractive radiation shed as the solitary wave evolves. Without proper inclusion of this radiation, the solitary waves do not evolve.

Besides accurately predicting the evolution of a dark or gray Kerr soliton, the modulation theory also gives good agreement with numerical solutions for the reorientational case, both for the steady-state nematicon and for its self-similar evolution. An unusual feature of the steady dark or gray nematicon is that its profile does not vary in a monotonic fashion to the background level, as does a dark or gray NLS soliton, but contains trapped linear modes at its tails, which take the form of humps. These humps are confined by the optic axis (director) distribution due to the nonlocal response of nematic liquid crystals, a feature missing in Kerr media described by the defocusing NLS equation. The trapped linear modes also presented challenges in terms of the appropriate definition and measurement of the nematicon width. The results of modulation theory appear to be in qualitative agreement with the first experimental results on dark nematicons, despite the fact that the actual material employed in the measurements exhibited a more complicated response than the purely reorientational one analyzed here [7]. Furthermore, studies of the interaction

of dark (grey) nematicons will enable us to better assess the consistency between modulation theory models and the response of reorientational media in the presence of resonant absorption and induced changes in order parameter.

ACKNOWLEDGMENT

This research was supported by the Royal Society of London under Grant No. JP090179.

APPENDIX: THE NUMERICAL SCHEME

The numerical solutions of the defocusing NLS or NLS-type equations (2) and (25) were obtained by using centered finite differences in the spatial coordinate x and a fourth-order Runge-Kutta method for the timelike, propagation direction z. This method was chosen over pure finite difference methods due to its high accuracy relative to computational cost. For the nematicon system, the solution of the director equation (26) was found using Gauss-Seidel iteration with successive over-relaxation. The Laplacian operator in Eq. (26) was discretized using central differences to ensure second-order accuracy.

The numerical solution method is described below for the defocusing nematicon equations (25) and (26). The defocusing NLS equation (2) is a special case with $\nu = 0$ and $q = 2$. Let us use the notation

$$\begin{aligned} u_{m,n} &= u(z_m = m\Delta z, x_n = n\Delta x), \\ \theta_{m,n} &= \theta(z_m = m\Delta z, x_n = n\Delta x), \end{aligned} \tag{A1}$$

$n = 1, \ldots, N$, $m = 1, 2, \ldots$, for the numerical solution. The nematicon equations can be written in the form of an ode by discretizing the x derivatives using centered differences to obtain

$$\begin{aligned} u_{mz} = f(u_{m,n}) = \frac{i}{2\Delta x^2}(u_{m,n+1} + u_{m,n-1} - 2u_{m,n}) \\ - i(u_{m,n+1} + u_{m,n-1})\theta_{m,n}(u_{m,n}). \end{aligned} \tag{A2}$$

The fourth-order Runge-Kutta method then gives the solution at z_{m+1} as

$$u_{m+1,n} = u_{m,n} + \tfrac{1}{6}(a_{m,n} + 2b_{m,n} + 2c_{m,n} + d_{m,n}), \tag{A3}$$

where

$$a_{m,n} = \Delta z f(u_{m,n}), \quad b_{m,n} = \Delta z f\left(u_{m,n} + \frac{a_{m,n}}{2}\right),$$

$$c_{m,n} = \Delta z f\left(u_{m,n} + \frac{b_{m,n}}{2}\right), \quad d_{m,n} = \Delta z f(u_{m,n} + c_{m,n}).$$

The function $f(u)$ in Eq. (A2) depends on u explicitly, and also implicitly via the director equation (26). To apply the Runge-Kutta method (A3) a solution is needed for the director distribution θ corresponding to a small change in u. This solution is found by solving

$$\nu\frac{\partial^2\theta}{\partial x^2} - 2q\theta = -2|u_{m,n} + \delta u|^2 \tag{A4}$$

to calculate the expressions for $b_{m,n}$, $c_{m,n}$, and $d_{m,n}$ at each z-step in the Runge-Kutta method. Once $u_{m+1,n}$ is found, the corresponding value of $\theta_{m+1,n}$ is calculated by solving (26). All applications of the Gauss-Seidel method needed only two iterations to obtain a converged solution due to the small value of Δz used. The accuracy of the numerical method at each z-step is $O(\Delta z^4, \Delta x^2)$.

[1] G. B. Whitham, *Linear and Nonlinear Waves* (John Wiley and Sons, New York, 1974).

[2] Y. S. Kivshar and G. P. Agrawal, *Optical Solitons: From Fibers to Photonic Crystals* (Academic Press, San Diego, 2003).

[3] G. Assanto and M. Karpierz, Liq. Cryst. **36**, 1161 (2009).

[4] C. Conti, M. Peccianti, and G. Assanto, Phys. Rev. Lett. **91**, 073901 (2003).

[5] G. Assanto, A. Minzoni, and N. F. Smyth, J. Nonlin. Opt. Phys. Mater. **18**, 657 (2009).

[6] C. Conti and G. Assanto, in *Encyclopedia of Modern Optics*, edited by R. D. Guenther, D. G. Steel, and L. Bayvel, Vol. 5 (Elsevier, Oxford, 2004), pp. 43–55.

[7] A. Piccardi, A. Alberucci, N. Tabiryan, and G. Assanto, Opt. Lett. **36**, 1356 (2011).

[8] W. L. Kath and N. F. Smyth, Phys. Rev. E **51**, 1484 (1995).

[9] A. A. Minzoni, N. F. Smyth, and A. L. Worthy, J. Opt. Soc. Am. B **24**, 1549 (2007).

[10] B. D. Skuse and N. F. Smyth, Phys. Rev. A **79**, 063806 (2009).

[11] G. Assanto, A. A. Minzoni, M. Peccianti, and N. F. Smyth, Phys. Rev. A **79**, 033837 (2009).

[12] G. Assanto, N. F. Smyth, and W. Xia, Phys. Rev. A **84**, 033818 (2011).

[13] G. Assanto, B. D. Skuse, and N. F. Smyth, Photon. Lett. Poland **1**, 154 (2009).

[14] G. Assanto, B. D. Skuse, and N. F. Smyth, Phys. Rev. A **81**, 063811 (2010).

[15] G. Assanto, A. A. Minzoni, N. F. Smyth, and A. L. Worthy, Phys. Rev. A **82**, 053843 (2010).

[16] G. Assanto, T. R. Marchant, and N. F. Smyth, Phys. Rev. A **78**, 063808 (2008).

[17] A. A. Minzoni, N. F. Smyth, A. L. Worthy, and Y. S. Kivshar, Phys. Rev. A **76**, 063803 (2007).

[18] Z. Xu, N. F. Smyth, A. A. Minzoni, and Y. S. Kivshar, Opt. Lett. **34**, 1414 (2009).

[19] A. A. Minzoni, N. F. Smyth, Z. Xu, and Y. S. Kivshar, Phys. Rev. A **79**, 063808 (2009).

[20] A. A. Minzoni, N. F. Smyth, and Z. Xu, Phys. Rev. A **81**, 033816 (2010).

[21] C. García-Reimbert, A. A. Minzoni, and N. F. Smyth, J. Opt. Soc. Am. B **23**, 294 (2006).

[22] Y. S. Kivshar and X. Yang, Phys. Rev. E **49**, 1657 (1994).

[23] Y. S. Kivshar and W. Krolikowski, Opt. Commun. **114**, 353 (1995).
[24] D. Anderson, Phys. Rev. A **27**, 3135 (1983).
[25] B. A. Malomed, Prog. Opt. **43**, 71 (2002).
[26] J. Yang, Stud. Appl. Math. **98**, 61 (1997).
[27] D. E. Pelinovsky and Y. Yang, Stud. Appl. Math. **105**, 245 (2000).
[28] M. J. Ablowitz, S. D. Dixon, T. P. Horikis, and D. J. Frantzeskakis, Proc. R. Soc. London A **467**, 2597 (2011).
[29] C. Conti, M. Peccianti, and G. Assanto, Phys. Rev. Lett. **92**, 113902 (2004).
[30] A. A. Minzoni, N. F. Smyth, and A. L. Worthy, Physica D **206**, 166 (2005).